Vertical dynamic measurements of a railway transition zone

a case study in Sweden

Unsiwilai, Siwarak; Shen, Chen; Zeng, Yuanchen; Wang, Li; Núñez, Alfredo; Li, Zili

Important note
To cite this publication, please use the final published version (if applicable).
Please check the document version above.

ORIGINAL PAPER

Vertical dynamic measurements of a railway transition zone: a case study in Sweden

Siwarak Unsiwilai[1] · Chen Shen[1] · Yuanchen Zeng[1] · Li Wang[1] · Alfredo Núñez[1] · Zili Li[1]

© The Author(s) 2024

Abstract

This study presents a measuring framework for railway transition zones using a case study on the Swedish line between Boden and Murjek. The final goal is to better understand the vertical dynamics of transition zones using hammer tests, falling weight measurements, and axle box acceleration (ABA) measurements. Frequency response functions (FRFs) from hammer tests indicate two track resonances, for which the FRF magnitudes on the plain track are at least 30% lower than those at the abutment. The falling weight measurements indicate that the track on the bridge has a much higher deflection than the track on the embankment. Two features from ABA signals, the dominant spatial frequency and the scale average wavelet power, show variation along the transition zone. These variations indicate differences in track conditions per location. Finally, the ABA features in the range of 1.05–2.86 m^{-1} are found to be related to the track resonance in the range of 30–60 Hz. The findings in this paper provide additional support for physically interpreting train-borne measurements for monitoring transition zones.

Keywords Railway transition zone · Railway track vertical dynamic · Axle box acceleration · Impact excitation · Railway bridge

1 Introduction

Railway transition zones are one of the most critical track segments in railway networks since they connect plain tracks and rigid structures, such as bridges, culverts, and tunnels. The differences in the track substructures at transition zones lead to fast track degradation due to the unevenness in the track support conditions [1–8]. Therefore, transition zones require more inspection and maintenance than plain tracks. In the Netherlands, maintenance activities at transition zones are reported to be at least twice as frequent as those conducted on plain tracks [9]. Furthermore, maintenance activities are expensive in terms of budget and human resources. In addition, track availability is reduced during maintenance due to track closure or train speed restrictions. Thus, more efficient maintenance methodologies, such as condition-based maintenance, are needed, for which frequent updates of crucial information on transition zone health conditions are necessary.

According to the literature, several wayside measurement techniques have been developed to evaluate the performance and monitor transition zone dynamic behavior. In [10], the performance of the transition zone measurement was investigated based on the vertical acceleration of sleepers under excitation when trains pass by. Transition zones with track geometry problems have sleeper accelerations that are approximately two times higher than those of a plain track. In [11], a framework that assesses the performance of a transition zone at a culvert was developed. The measurements consist of the track dynamic flexibility based on hammer tests and responses of track components to traffic

✉ Zili Li
  Z.Li@tudelft.nl

  Siwarak Unsiwilai
  S.Unsiwilai@tudelft.nl

  Chen Shen
  C.Shen-2@tudelft.nl

  Yuanchen Zeng
  Y.Zeng-2@tudelft.nl

  Li Wang
  L.Wang-7@tudelft.nl

  Alfredo Núñez
  A.A.NunezVicencio@tudelft.nl

1   Section of Railway Engineering, Department of Engineering Structures, Faculty of Civil Engineering and Geosciences, Delft University of Technology, Stevinweg 1, 2628 CN Delft, The Netherlands
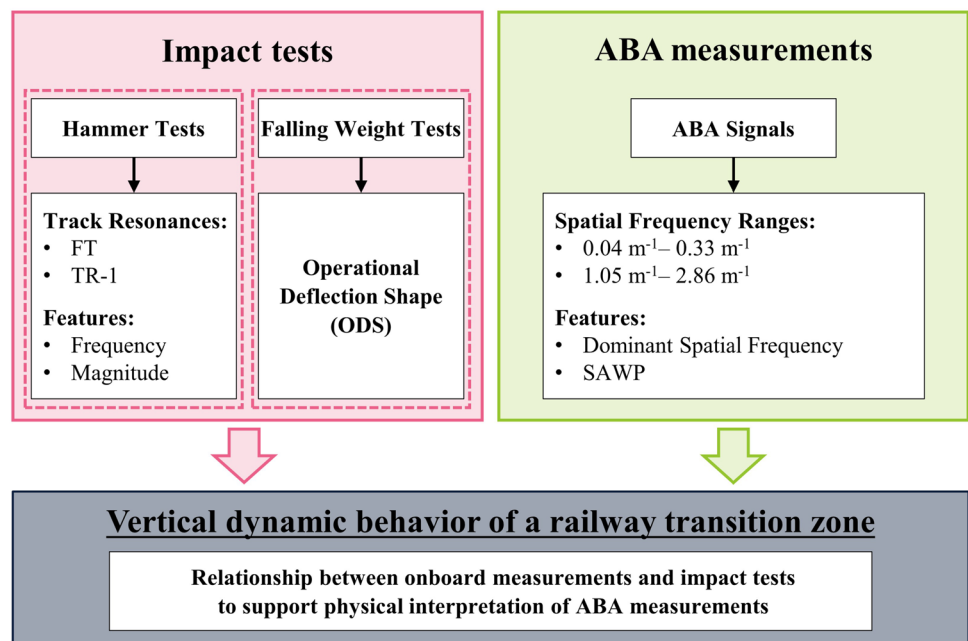
loads. The results showed that the track on the culvert provided 60% less track dynamic flexibility and 45% lower track displacement than plain tracks. In [12], the root cause of differential displacements at transition zones was investigated. Poor sleeper support conditions were found to be a direct cause of the permanent deformation of the transition zones. In [13], the settlement of multiple substructure layers at transition zones was monitored using multidepth deflectometers (MDDs). The ballast layer exhibited the most accumulated permanent and transient deformations in the case studied. From the literature, wayside measurement techniques have been able to provide different types of information on transition zones. However, track access, the availability of power supplies, human resources, and budgets are significant limitations in deploying wayside measurements.

Onboard sensing solutions have been proposed in the literature for monitoring track geometry degradation in transition zones. For example, the track quality and ride comfort at transition zones have been analyzed using acceleration measured by smartphones [14]. In [15], track vertical displacement due to different loading conditions in transition zones was measured using a mobile system called the rail infrastructure alignment acquisition (RILA) system. In our previous work [16], key performance indicators (KPIs) for monitoring transition zones were proposed from wavelet-based features of axle box acceleration (ABA) signals. Nevertheless, further understanding of train-track dynamics at transition zones is needed to increase the interpretability of ABA responses and KPIs for condition assessment. This paper contributes to filling this research gap by proposing and applying a measurement framework that combines trackside and train-borne

technologies for characterizing the vertical dynamic behavior of a railway transition zone. First, two impact excitation tests, namely hammer tests and falling weight tests, are conducted trackside. Frequency response functions (FRFs) regarding the impact force and track component responses are obtained to characterize the track deflection and track resonances (TRs). Variations in the frequency and magnitude features of the FRFs per location indicate the differences in track conditions. Then, train-borne ABA measurements are conducted, and two wavelet-based features at two spatial frequency ranges (0.04–0.33 m^{-1} and 1.05–2.86 m^{-1}), dominant spatial frequency and the scale average wavelet power (SAWP), are extracted from the vertical ABA signals. Variations in wavelet-based features are found along the transition zone, indicating changes in track conditions. Further, the ABA features are compared with the features from the impact excitation tests. The ABA features in the spatial frequency range of 1.05–2.86 m^{-1} align well with the FRF features at the full track resonance (FT). Their relationship provides experimental evidence on the train-track-embankment vertical dynamic behavior and increases the interpretability of the ABA responses in assessing track conditions. Figure 1 describes the flowchart of the proposed measuring framework.

The remaining parts of this paper are organized as follows. First, a case study transition zone and the measurement campaign for track vertical response identification are described in Sect. 2. In Sect. 3, the analyses of the track vertical responses from hammer tests and falling weight tests are described. Then, an analysis of the ABA responses at the transition zone is presented in Sect. 4. In Sect. 5, findings

Fig. 1 Flowchart of the proposed framework of this study

Impact tests

- Hammer Tests
  - Track Resonances:
    - FT
    - TR-1
  - Features:
    - Frequency
    - Magnitude
- Falling Weight Tests
  - Operational Deflection Shape (ODS)

ABA measurements

- ABA Signals
  - Spatial Frequency Ranges:
    - 0.04 m^{-1}– 0.33 m^{-1}
    - 1.05 m^{-1}– 2.86 m^{-1}
  - Features:
    - Dominant Spatial Frequency
    - SAWP

Vertical dynamic behavior of a railway transition zone

Relationship between onboard measurements and impact tests to support physical interpretation of ABA measurements

from the relationship between the impact excitation tests and ABA signals are discussed. Finally, conclusions and suggestions for further studies are presented in Sect. 6.

2 Measurements for track vertical dynamic analysis at transition zones

2.1 Description of the case study

The railway transition zone analyzed in this paper is located at a single-span bridge in the Iron Ore Line of Sweden between Boden station and Murjek station. The railway line is a single ballasted-track with passenger and freight traffic, including iron ore trains with the heaviest axle load of more than 30 tons. Figure 2 shows the bridge and its transition zones.

This bridge is 8.15 m long and has one span, comprising a 4.2 m bridge deck (Zone B), a 1.9 m north approach slab (Zone A), and a 2.05 m south approach slab (Zone C). It is noted that cracks are found on the bridge abutments, which are evidence of the degradation of the bridge structure. Hence, this bridge was strengthened by installing two steel beams spaced 2.6 m apart to support the bridge deck.

2.2 Impact excitation tests

Impact excitation tests are a common nondestructive measurement technique that is used to identify the dynamic behaviors of a structure by investigating features of their frequency response functions (FRFs). FRFs are transfer functions of the responses of a structure (output) to an impact excitation (input). According to the literature, dynamic characteristic identification [17–19] and estimation of the track component parameters [20, 21] can be made by investigating the features of the FRFs. In this study, we consider the impact force, $F(t)$, applied on the rail head as the input and the acceleration, $a(t)$, measured at either a rail or a sleeper as the output. The impact force must be controlled to prevent exceeding the measurement range of load cells and accelerometers. At the same time, excessive force that causes damage to the impactor, the sensors, or the structure at the impact location should also be avoided. In addition, following standard practice, multiple impacts are performed, and inadequate results are disregarded by the repeatability of both input and output signals. This procedure reduces uncertainties in FRF results from measurements.

Three types of FRFs are assessed: accelerance, mobility, and receptance, whose descriptions and relationships are given in Table 1 [22]. In the table, $S_{aF}(f)$ is the

Fig. 2 A case study track at a short single span bridge: **a** a top view satellite photo. (source: Google Maps); **b** a front view photo; **c** a side view photo
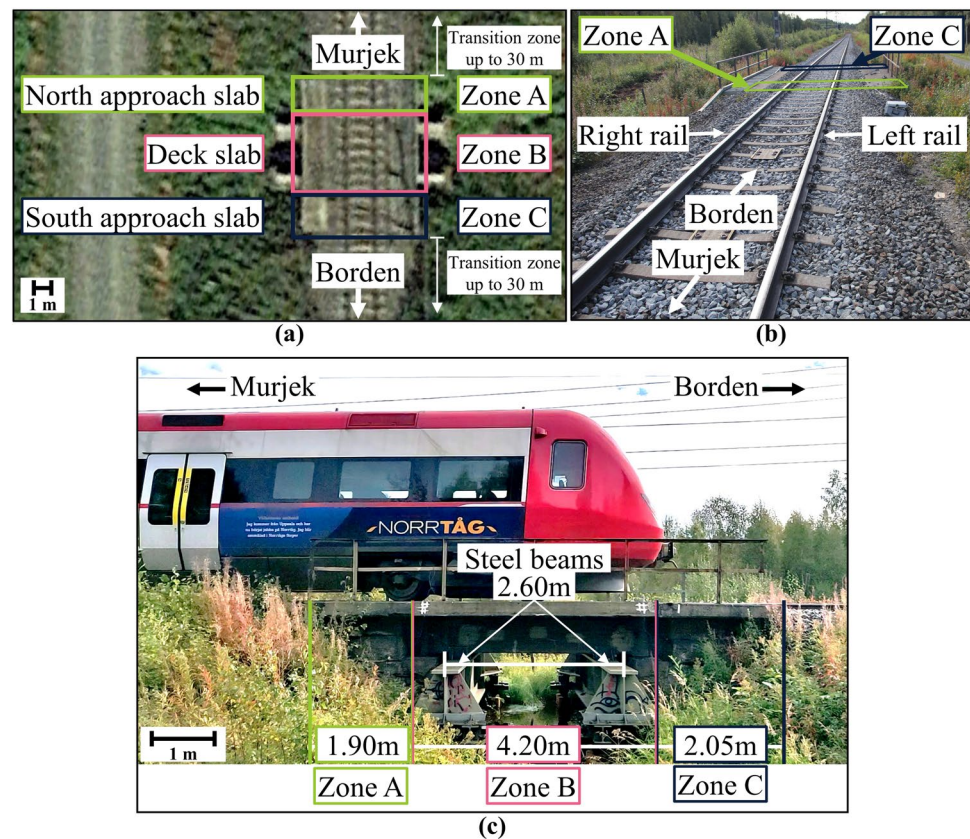
Table 1 Frequency response functions and their relationship (modified from [22])

Types of FRFs	Accelerance, $H_a(f)$	Mobility, $H_v(f)$	Receptance, $H_d(f)$
Definition	$\dfrac{\text{Acceleration}}{\text{Force}}$	$\dfrac{\text{Velocity}}{\text{Force}}$	$\dfrac{\text{Displacement}}{\text{Force}}$
Formula	$H_a(f) = \dfrac{S_{aF}(f)}{S_{FF}(f)}$	$H_v(f) = \dfrac{H_a(f)}{2\pi f}$	$H_d(f) = \dfrac{H_v(f)}{2\pi f}$

cross-spectrum of the force and the acceleration, $S_{FF}(f)$ is the autospectrum of the force, and f is the frequency.

By analyzing the peaks of the FRFs, it is possible to identify the track resonances (TRs) [18, 22]. By observing a specific TR, the deviation in both the frequency and magnitude suggests differences in the dynamic characteristics of the railway track system. Furthermore, different track components have their respective characteristic frequency ranges. For example, track substructure components generally correspond to a frequency range below 150 Hz [23], while track responses in a frequency range from 150 to 800 Hz are

mainly related to sleepers, fastening systems, and rails [24]. In this study, we conducted two types of impact excitations: (1) hammer tests that are suitable to obtain reliable track responses in the frequency range from 30 to 500 Hz and (2) falling weight tests that reliably obtain track responses in the frequency range from 10 to 100 Hz. More details can be found in the following subsections. In this study, the reference position (0 m) was defined at the outer edge of the north approach slab, and the position increases in the direction of Boden station. The average distance of the sleeper interval is 0.65 m. Figure 3 shows the locations where hammer tests were conducted on the rail head above sleepers sp_1 to sp_{10} and the locations of accelerometers a_1 to a_8 for track response measurement during the falling weight tests.

2.2.1 Hammer tests

Hammer tests were conducted at 10 locations corresponding to the locations of consecutive sleepers, covering one transition zone (embankment and north abutment). Sleepers sp_1
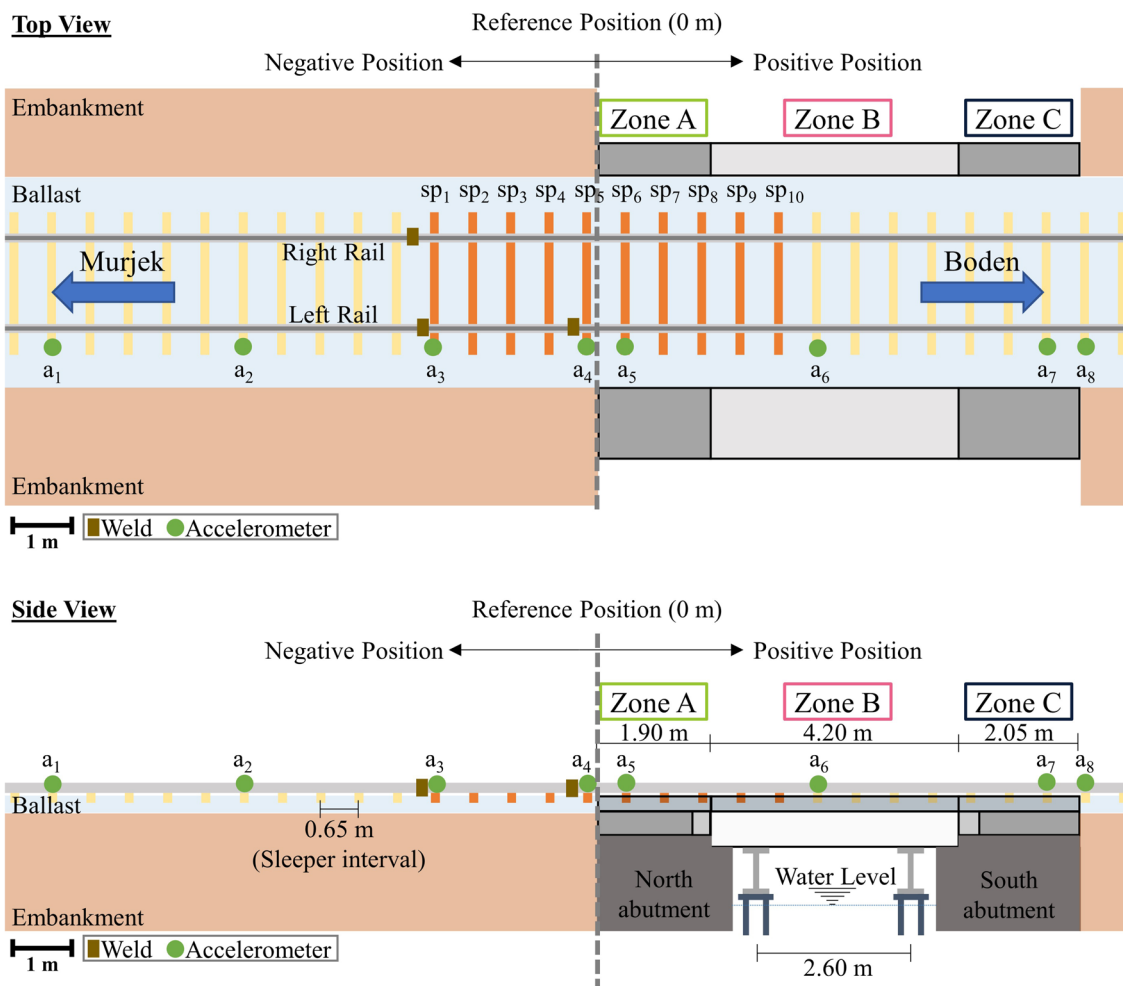
Fig. 3 Reference position, hammer test locations, and accelerometer positions

to sp_5 are located on the track segment on the embankment, while sleepers sp_6 to sp_{10} are located on the segment on the bridge structure. We investigate 'on-support' track responses by applying the impact excitation using a 5.5 kg hammer (PCB 086D50, measurement range: 0–22.2 kN) with a plastic, flat surface, 76 mm in diameter, as a hammer tip on the left rail head directly above the sleeper as an input. The output is a response of the track system in the vertical direction, measured using a unidirectional accelerometer (Brüel & Kjaer 4514-004, measurement range: ± 980 m/s^2), named a_r, attached to the rail head close to the impact location. The force and acceleration signals were recorded using a data acquisition system (MBBM PAK MKII) at a sampling rate of 25.6 kHz. Several impact tests were conducted at the rail head above a particular sleeper. Then, five impacts that provide good coherence were used to calculate an average FRF for minimizing random errors. This setup is shown in Fig. 4.

2.2.2 Falling weight tests

Falling weight tests efficiently apply large impact energy to the track system to obtain substructure component responses. A special apparatus was designed to release the stacked weight with a plastic, flat surface, 76 mm in diameter, as a tip, similar to a hammer tip, in which the weight and dropping height are adjustable. The impact force is measured using a load cell (Omega LCWD-100 K, measurement range: 0–444.4 kN). In this study, the impact location is at the left rail head at the reference position (0 m) between sp_5 and sp_6. Weights of 60 kg, 80 kg, and 100 kg were dropped from 27 cm, 37 cm, and 47 cm above the rail head. Six unidirectional accelerometers (Bruel & Kjaer 4514-004, measurement range: ± 980 m/s^2), a_1 to a_3 and a_6 to

a_8, and two three-directional accelerometers (PCB 356B21, measurement range: ± 4905 m/s^2), a_4 and a_5 (closest sleepers to the impact location), were attached to the sleepers for measuring transition zone responses. Figure 5 shows the measurement setup. The force and acceleration signals were recorded and synchronized using a data acquisition system (MBBM PAK MKII) at a sampling rate of 25.6 kHz. Finally, the average FRF at a particular accelerometer location is calculated using the input and output from 9 configurations of impact (Fig. 6).

2.3 Axle box acceleration measurement system

An ABA measurement system was designed to measure vehicle responses on axle boxes as the vehicle interacts with the track. In this study, such a system was installed in a passenger wagon. At each axle box, responses were measured using unidirectional accelerometers. In addition, the train position and speed were measured using a high-precision GPS receiver module. All signals were synchronized and recorded using a data acquisition system (NI compact RIO) at a sampling rate of 25.6 kHz. More details of the ABA measurement system can be found in [25, 26].

In this paper, we consider vertical ABA signals. The acceleration at time instant t for wheelset w and rail r is defined as $a_{w,r}(t)$. Eight acceleration signals from four wheelsets $w \in \{1, 2, 3, 4\}$ and the left (L) and right (R) rails $r \in \{L, R\}$ are considered. The location of wheelset w at time instant t is $x_w(t)$. Then, after synchronizing the signals, the acceleration signals can be evaluated as a function of the track location x, $a_{w,r}(x)$.

The wavelet power spectrum (WPS), which is the product of the continuous wavelet transform (CWT), is considered for
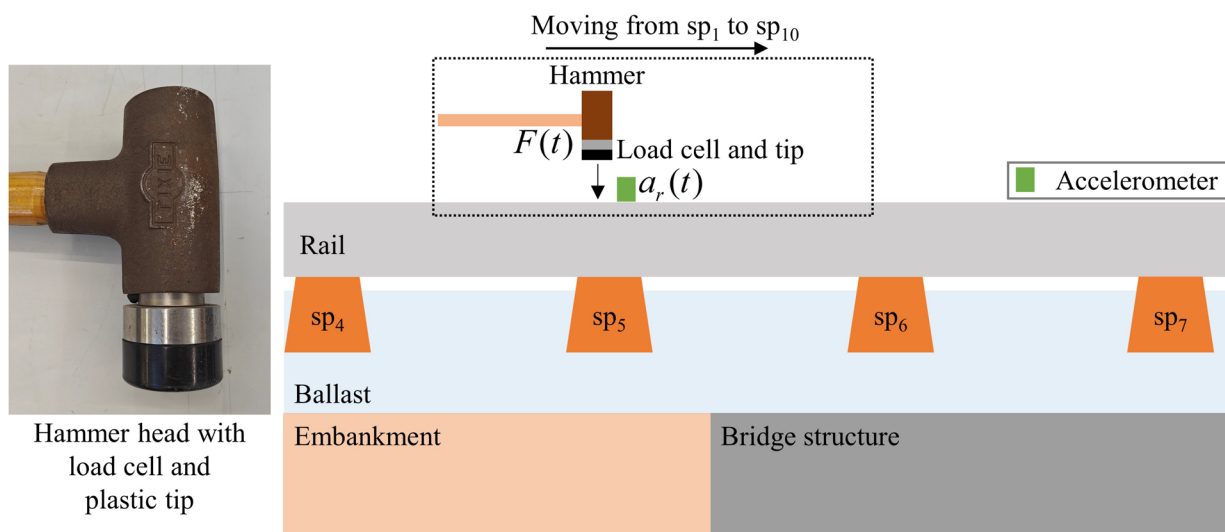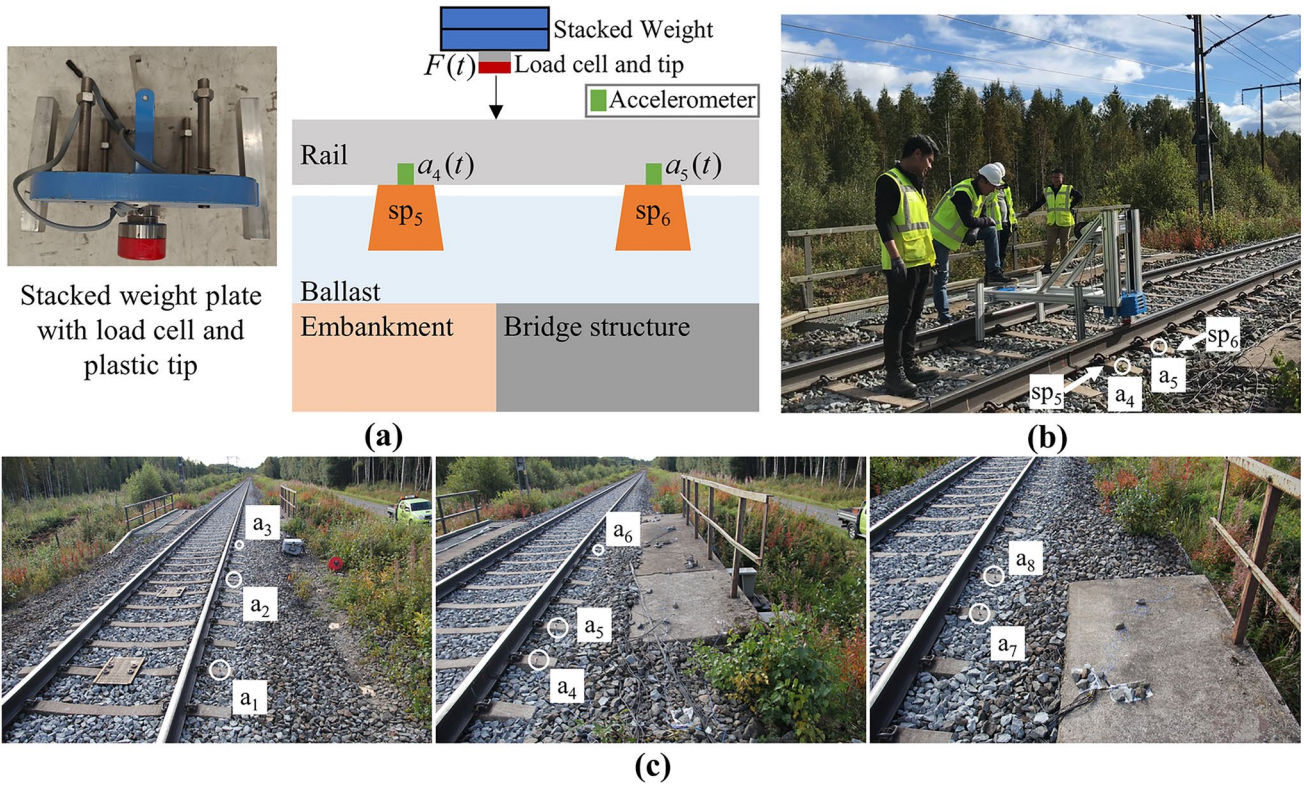

Fig. 4 A schematic diagram of the hammer test

Fig. 5 Falling weight impact test: **a** a schematic diagram; **b** the falling weight release equipment; **c** accelerometers at eight considered locations
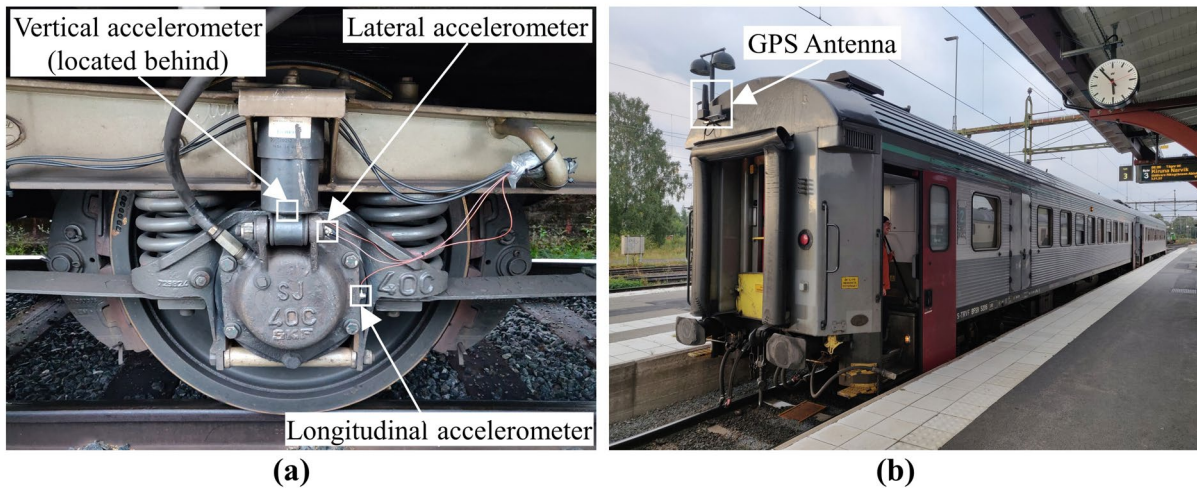

Fig. 6 ABA measurement system setup on a passenger wagon: **a** position of the accelerometers at one of eight axle boxes; **b** GPS antenna on the roof of the passenger wagon

analyzing the variation of ABA signals in the time–frequency domain. The WPS can be calculated as follows [27]:

$$\text{WPS}_{w,r}(x, s) = \left| \sum_{n'=0}^{N-1} a_{w,r}(n') \psi^* \left(\frac{(n' - n)\delta_t}{s} \right) \right|^2 \tag{1}$$

where $\text{WPS}_{w,r}(x, s)$ is the WPS of the acceleration signal from wheel w and rail r at location x and wavelet scale s with $s > 0$. N is the number of data points in a considered time frame, $n' = 0, ..., N - 1$, $a_{w,r}(n')$ is the ABA signal at an instant $x_w(n')$, n is the time index variable for the continuous translation, δ_t is the time interval between data points, and ψ is the wavelet mother function. The function $\psi *$ is a family of wavelets derived from the mother wavelet by translations and scaling, and $*$ refers to the complex conjugate. We used the Morlet function as the mother wavelet for this study.

Then, two features can be extracted from the WPS, the global wavelet power spectrum (GWPS) and the scale average wavelet power (SAWP), to investigate distributions of the WPS in the frequency (scale) domain and the space domain, respectively.

The GWPS can be calculated as follows [27]:

$$\text{GWPS}_{w,r}(s) = \frac{1}{n_2 - n_1} \sum_{n=n_1}^{n_2} \text{WPS}_{w,r}(x(n), s), \quad x(n_1) < x(n) < x(n_2) \tag{2}$$

where $\text{GWPS}_{w,r}(s)$ is the GWPS of the acceleration signal from wheel w and rail r within the location from $x(n_1)$ to $x(n_2)$ for wavelet scale s with $s > 0$, $\text{WPS}_{w,r}(x(n), s)$ is the wavelet power spectrum at position $x(n)$ and scale s, and n_1 and n_2 are selected according to the preferred length of track segment in the analysis. The track segment length can be adjusted based on user preference. The longer considered track segment makes the dominant spatial frequency more pronounced; however, the local characteristics will be hindered. In addition, the number of data points per considered segment depends on measurement speed since the ABA measurement system records signals with a fixed sampling rate. The lower speed provides a higher number of data points.

This study investigates the variation of track characteristics on the sleeper interval basis. Therefore, we considered the number of data points corresponding to the measurement speed and the spacing between sleepers at 0.65 m for determining the dominant spatial frequency in Sect. 4.2.

The SAWP can be calculated as follows [27]:

$$\text{SAWP}_{w,r}(x) = \frac{\delta_j \delta_t}{C_\delta} \sum_{j=j_1}^{j_2} \frac{\text{WPS}_{w,r}(x, s_j)}{s_j} \tag{3}$$

where $\text{SAWP}_{w,r}(x)$ is the SAWP of the acceleration signal from wheel w and rail r at location x within wavelet scale s from s_{j_1} to s_{j_2}, $\text{WPS}_{w,r}(x, s_j)$ is the wavelet power spectrum at scale j, δ_j is the scale step, δ_t is the time step, and C_δ is the empirically derived constant of the wavelet function.

3 Characteristics of the transition zone responses to impact excitation tests

3.1 Identification of the reliable frequency range

We identify the reliable frequency range of FRFs based on two criteria [20]: 1) the variance of the FRFs for different impact tests should be small, which means there is a narrow envelope in the reliable frequency range, and 2) the coherence should be close to 1 in the reliable frequency range. The coherence is a statistical value in a function of frequency that examines the relation between the input signal (the impact force, $F(t)$) and the output signal (the acceleration, $a(t)$), ranging from 0 to 1. At a considered frequency, the coherence close to 1 indicates a strong relationship between input and output signals. Hence, the quality of the FRF can be indicated by the coherence. The coherence can be calculated as follows:

$$C_{aF}(f) = \frac{\left| S_{aF}(f) \right|^2}{S_{aa}(f) S_{FF}(f)} \tag{4}$$

where $C_{aF}(f)$ is the coherence, $S_{aF}(f)$ is the cross-spectrum of the force and the acceleration, $S_{aa}(f)$ is the autospectrum of the acceleration, $S_{FF}(f)$ is the autospectrum of the force, and f is the frequency.

We chose the FRFs for the hammer tests at the location of sleeper sp_1 as an example. The average FRF, including the envelope (maximum and minimum values) and the coherence, are shown in Fig. 7. Based on the mentioned criteria, while considering the FRFs at the ten different impact locations, it can be determined that the reliable frequency range is between 30 and 500 Hz.

Then, the reliable frequency range of the falling weight tests is determined. The responses of sleeper sp_5 are selected as an example since its distance from the impact locations of the hammer tests is 0.15 m, which can be considered minor. Based on the abovementioned criteria for determining a reliable frequency range, the results in Fig. 8c show that falling weight tests can be considered reliable from 10 to 100 Hz. Then, in the same figure, we compare the mobility functions between the two types of impact tests. Note that an additional peak of approximately 15 Hz is only observed from the mobility function from falling weight tests. The following peaks of approximately 50 Hz can be found from both falling weight and hammer tests, even though impact forces and accelerations from both impact tests are largely different,

Fig. 7 Hammer tests, responses measured at the rail head above sp$_1$: **a** an example of the impact force and the acceleration; **b** mobility and coherence of the track system from 5 hammer impacts
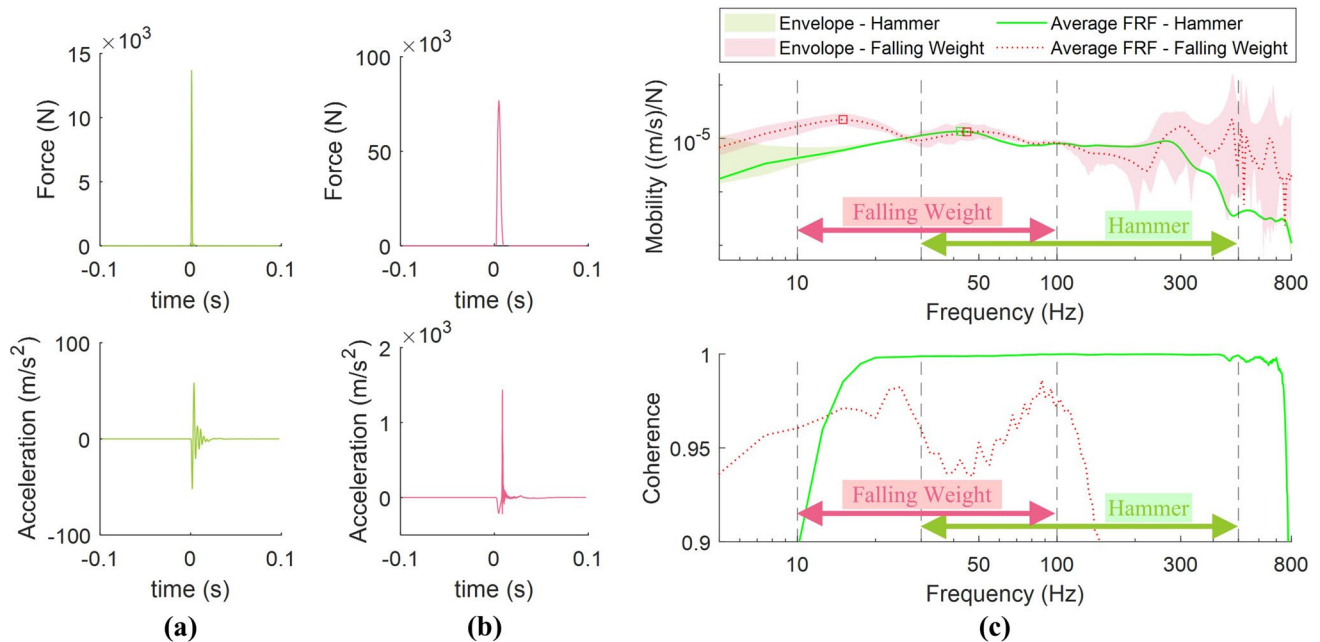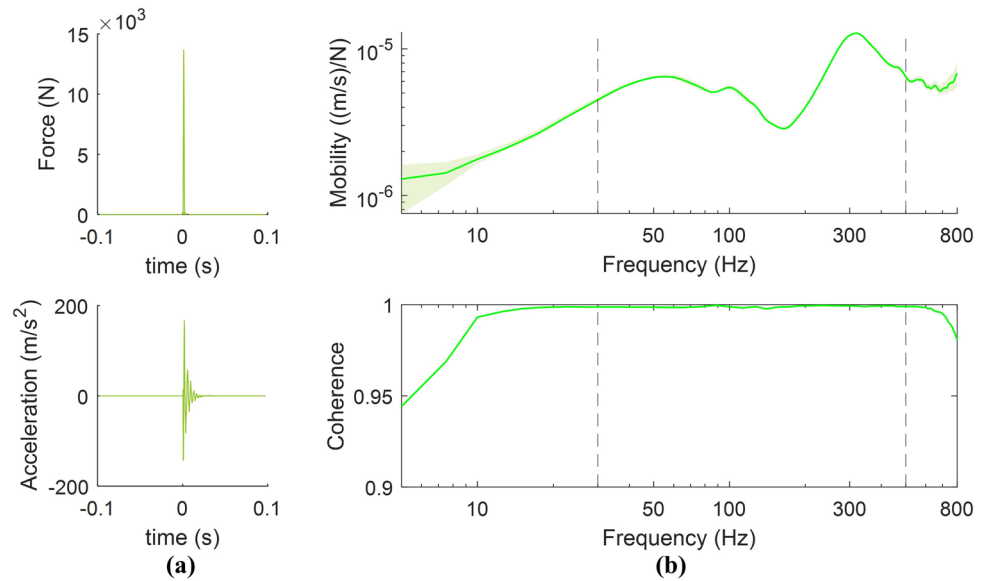

Fig. 8 Hammer test and falling weight test, responses measured at sleeper sp$_5$: **a** an example of the impact force and the acceleration due to a hammer impact; **b** an example of the impact force and the acceleration from a 100 kg weight dropped from 47 cm above the rail head; **c** mobility and coherence of the track system from ham-

mer test and falling weight test, □ indicates peaks. The envelope and the coherence of the hammer test are obtained for five impacts from a similar procedure, while the envelope of the falling weight considers a wider range of tests, including tests with different heights and weights

as shown in Fig. 8a and b. This finding suggests that the FRFs calculated from a wide range of input and output from different impact methods can identify track resonances as long as track resonances are within the reliable frequency range of those impact methods.

3.2 Vertical dynamic responses based on hammer tests

Figure 9a shows the mobility functions of hammer tests at sp$_1$ to sp$_{10}$, in which two noticeable peaks can be observed. The
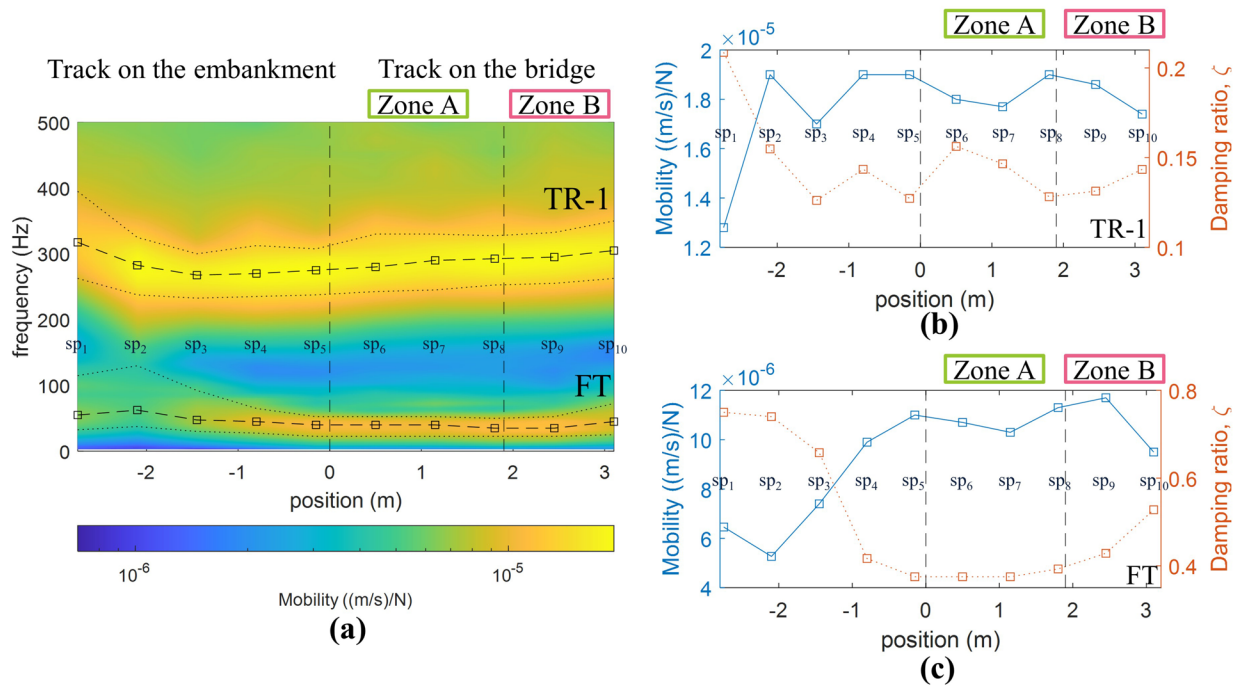
Fig. 9 Variation in FT and TR-1: **a** a surface plot of the FRFs, including the dropped 3 dB band; **b** mobility magnitude and damping ratio of TR-1; **c** mobility magnitude and damping ratio of FT. □ indicates the positions of sleepers sp_1-sp_{10}, from left to right
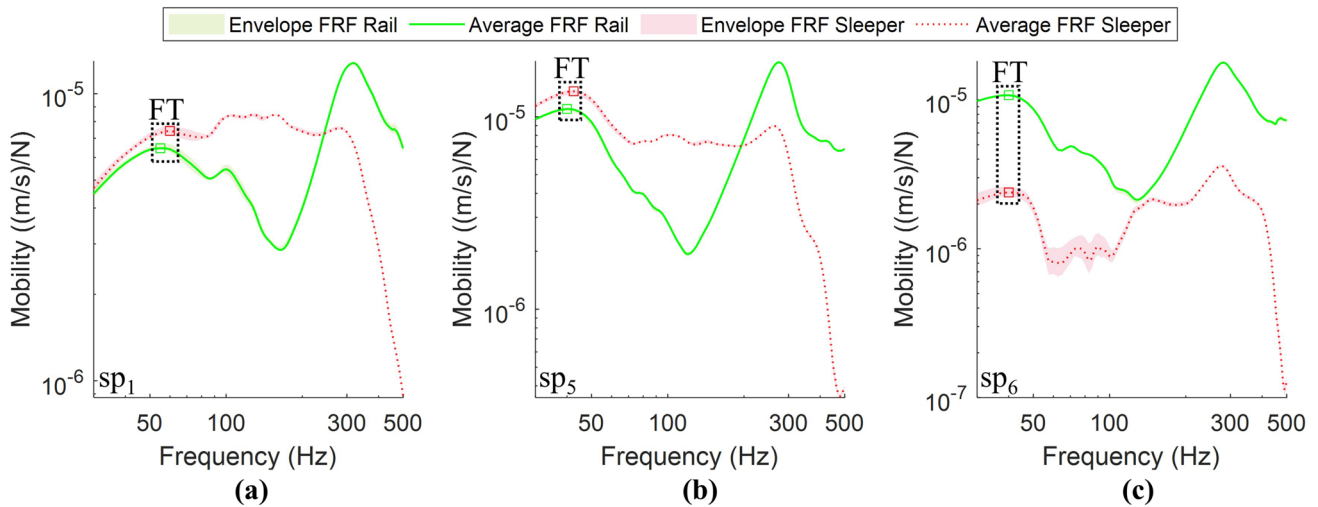
Fig. 10 FRFs of the track system with respect to responses at the rail head and the sleeper, □ indicates FT: **a–c** tests at the locations of sp_1, sp_5, and sp_6, respectively

first peak is in the range of approximately 30–60 Hz, and the second peak is in the range of approximately 270–320 Hz. The first peak is likely full track (FT) resonance, in which the rail and the sleeper vibrate together as a rigid body [22, 28]. The identification of the FT resonance can be explained by observing the mobility functions of two outputs at the rail head and underneath the sleeper with respect to the same input. Figure 10 compares the mobility functions of the rail

and the sleeper at 3 locations: sp1 (a_r and a_3), sp5 (a_r and a_4), and sp6 (a_r and a_5). In each subplot, the peak frequency values in the FT range are insignificantly different between the rail and sleeper FRFs, indicating that both components vibrate together at this resonance. The second peak is named TR-1, which could be related to the responses of other track components above a ballast layer. According to the literature, three track resonances can be determined by hammer tests: (1)

FT resonance, (2) rail resonance, in which the rail vibration is relative to the sleeper, and (3) pin-pin resonance, in which the track vibration wavelengths are equal to the sleeper spacing [22, 28]. Since the pin-pin resonance mostly occurs between 400 and 1200 Hz, TR-1 should be the rail resonance. Further experiments might be needed to prove this statement.

According to Fig. 9a, frequency shifting of FT and TR-1 can be observed from outside the bridge to inside the bridge. Additionally, Fig. 9b and c show variations in the magnitudes and damping ratio of TR-1 and FT along the considered track segment. The damping ratio (ζ) can be calculated as follows:

$$\zeta = \frac{\Delta f_{3dB}}{2f_0} \tag{5}$$

where ζ is the damping ratio, f_0 is the resonant frequency, and Δf_{3dB} is the bandwidth of the dropped 3 dB band from the resonant frequency. Given that the two considered locations provide similar resonant frequencies but differ in dropped 3 dB bandwidth. A location with a broader bandwidth represents a faster decay due to a higher damping characteristic, resulting in a higher damping ratio.

Considering the track segment on the embankment, the locations of sp_1, sp_2, and sp_3 show slightly higher FT frequency values than sp_4 and sp_5, while the corresponding mobility magnitudes are 40–55% lower. The damping ratio values at sp_1, sp_2, and sp_3 are 60–87% higher than sp_4 and sp_5, representing a faster acceleration decay due to higher damping. The differences in the local conditions in terms of stiffness and damping of the ballast layer should be key factors of the variations in the features of FT resonance [20, 22].

Regarding TR-1, the location of sp_1 shows a higher frequency value, but its mobility magnitude and damping ratio are approximately 30% lower and 50% higher than those at sp_2–sp_5, respectively. These findings indicate the different dynamic behavior of the track components above a ballast layer, and the influence of the nearby weld might have played a role.

While considering the track segment on the bridge from sp_6–sp_{10}, variations in the FT and TR-1 frequency, corresponding magnitudes, and damping ratio are minor compared to those on the embankment. These variations in FRF features from sp_1 to sp_{10} indicate how the vertical dynamic behavior of the track system changes as a function of the position along a transition zone.

3.3 Vertical dynamic responses based on falling weight tests

Different impact test configurations influence the characteristics of FRFs [17, 22]. For example, different FRFs are obtained when using different impact excitation forces (different hammers, heights, and weights of the falling weight device), different locations of interest of the output (rail or sleeper), and different distances between the input and output sensors. For example, the peak at 15 Hz (lower than the FT resonance) can be clearly observed from the FRFs of accelerometer a4, which is closest to the impact location, as shown in Fig. 8. However, FRFs with output sensors farther from the impact location of the falling weight do not obviously identify this peak. This peak could be related to the resonance of the track components underneath the ballast layer since the falling weight device provides higher excitation energy so that lower track components are more excited than when using the hammer.

In this section, we evaluate the deflection characteristics of the transition zone with falling weight at the reference location. We consider the sleeper responses for different frequency ranges through operational deflection shapes (ODSs). The ODS can be used to visualize the actual motion of the structure at the considered frequency, which can resemble mode shapes if the considered frequencies are close to the resonance frequencies of the system. The ODS of the instrumented track can be obtained by considering the imaginary parts of the FRFs, for which the receptance function is considered as follows [29]:

$$ODS(f) = \left[Im(FRF_{a_1}(f)), Im(FRF_{a_2}(f)), \dots, Im(FRF_{a_8}(f)) \right] \tag{6}$$

where $ODS(f)$ is the ODS of the track at the considered frequency f, and FRF_{a_i} is the receptance function of accelerometer a_i.

The ODS plots corresponding to the reliable frequency range of the falling weight tests from 10 to 100 Hz are shown in Fig. 11. Figure 11a shows the ODSs corresponding to the frequency range below the FT resonance, which could be related to the responses of the track components below the ballast layer. Except the responses of a4 at − 0.15 m, which provides the most deflection because it is closest to the impact load, it can be considered that the track segment on the embankment has less deflection than the track segment on the bridge, reflecting the higher capability of the embankment to dissipate and transmit energy compared to that of the track on the bridge. Looking at the ODSs in Fig. 11b, which are in the same frequency range as the FT resonance, the a_6 responses at 3.75 m provide the highest downward deflection. As seen in the ODSs in Fig. 11c, this location shows the highest upward deflection in the range between 60 and 100 Hz. The location of a_6 is close to the middle span of the bridge deck slab (Zone B); hence, this location can deflect more than Zone A and Zone C, which are closer to the abutments.

Fig. 11 Operational deflection shapes of the track at different corresponding frequencies: **a** 10–30 Hz; **b** 30–60 Hz; **c** 60–100 Hz. □ from left to right, indicate the positions of accelerometer a_1 to a_8, respectively, and the arrows represent the impact location at 0 m
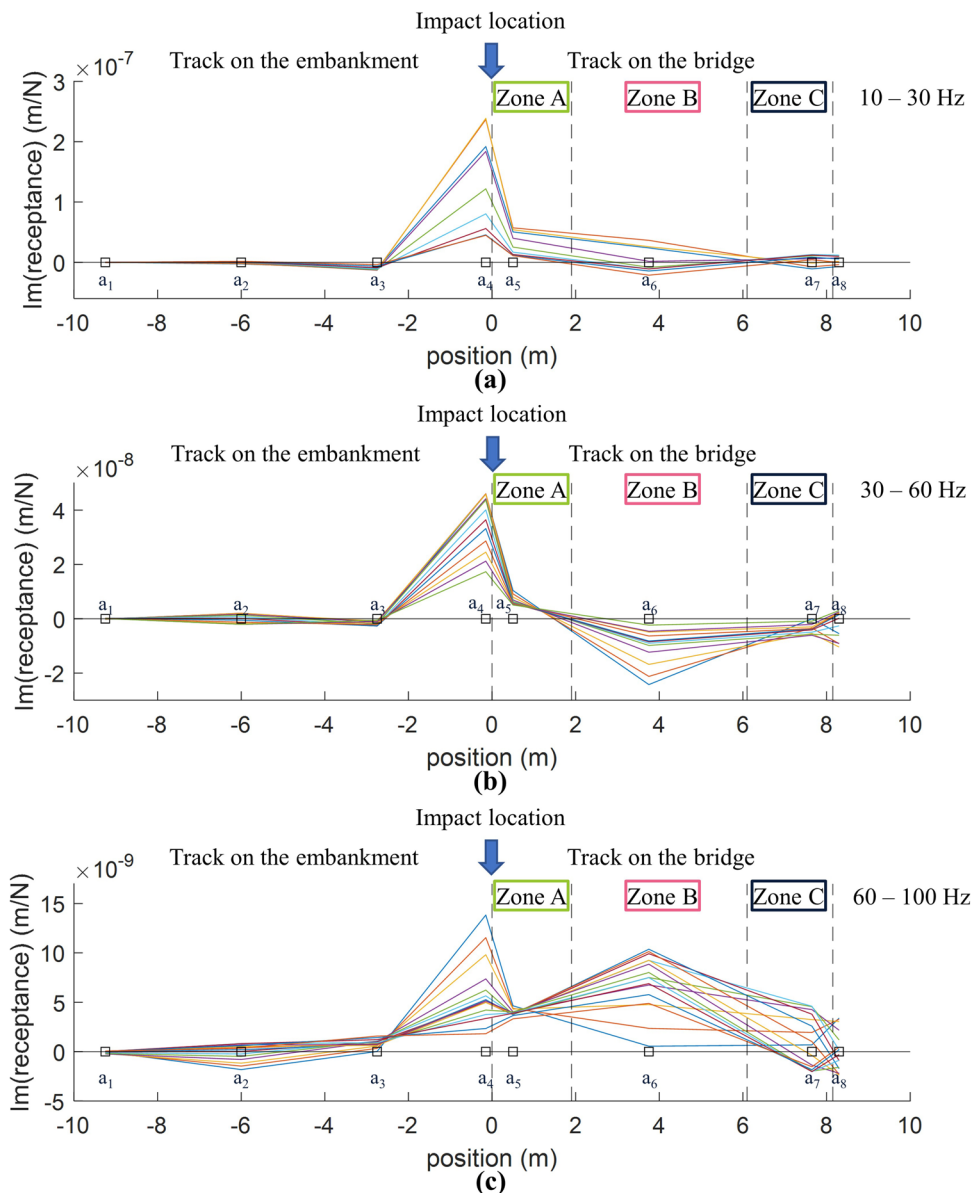
4 ABA responses at transition zones

4.1 ABA signals in the space domain and the space-spatial frequency domain

The ABA measurement system was deployed on 25 and 27 August 2022. Each day, the instrumented wagon passed by the case study transition zone two times in different directions. In total, the ABA signals from 4 measurements are available for analysis. Following the findings from a previous study [16], we consider the average vertical ABA signals from four axle boxes on the same side of the wagon and signals within 30 m from the abutment. Hence, the ABA responses from − 30.0 m to 38.15 m are considered in this study. Additionally, since the ABA responses are dependent

Table 2 The average speeds of the instrumented wagon while passing the studied transition zone

Average speed while passing the transition zone	Direction	
	To Murjek	To Boden
Day 1	31.7 m/s	26.8 m/s
Day 2	33.7 m/s	33.0 m/s

on the speed, we analyze the ABA responses in the space-spatial frequency domain instead of the time–frequency domain. The speed of the train during the different measurements varies, as shown in Table 2.

Figure 12 shows an example of the ABA signals measured toward Murjek station on day 1. Signals in the space domain
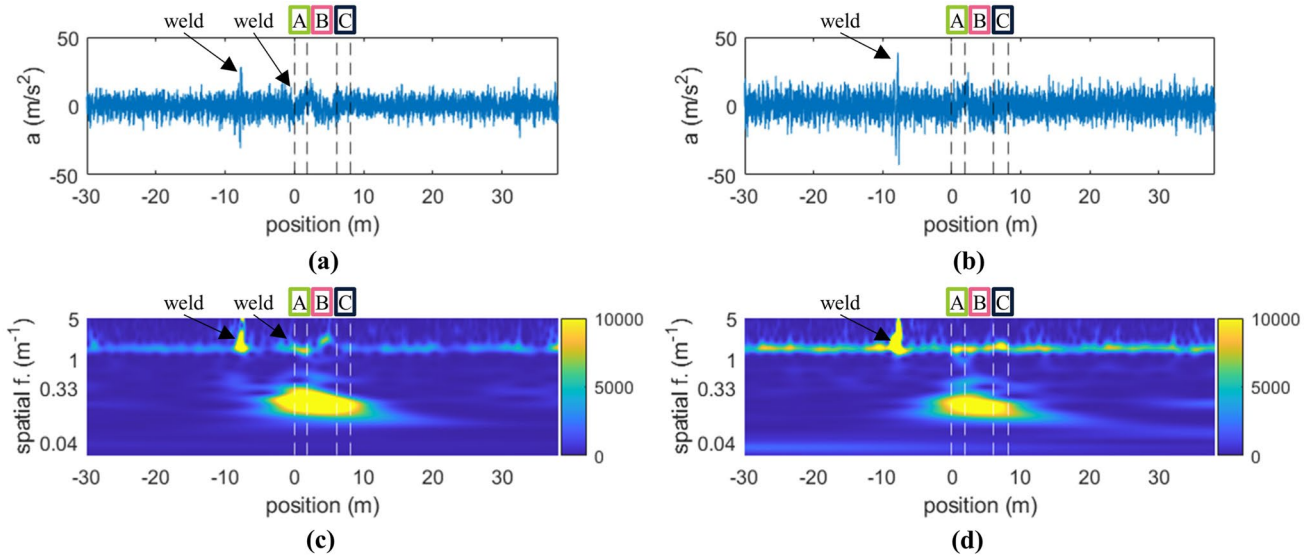
Fig. 12 Average ABA: **a**, **b** signals in the time domain on the left and right rails, respectively; **c**, **d** wavelet power spectra in the space-spatial frequency domain on the left and right rails, respectively

and the space–spatial frequency domain reflect the properties of the transition zone. Significant changes in ABA signals, particularly in the space-spatial frequency domain, can be observed. The high-energy area is noticed from Zone A to Zone C, with the highest spatial frequency of approximately 0.20 m^{-1} (equivalent to 5 m). This response relates to the interaction of the instrumented wagon with the bridge, and the noticeable spatial frequency is closely related to the length of the bridge deck, which is 4.20 m. Then, energy continuously decreases in the locations further away from the bridge, indicating a change due to the transition zones. Note that at -7.7 m, the spikes in the space domain signal and the high-energy area of approximately 1.53 m^{-1} (equivalent to 0.65 m) and higher are related to welds on both rails. However, the weld on the left rail at -0.3 m does not cause significant differences in the ABA signals. These characteristics of ABA signals regarding two welds could indicate differences in the weld health conditions, which further investigation could provide more understanding.

The developed KPI$^{\text{side}}$ [16] can be used to evaluate the difference in the degradation level between the transition zones of a bridge. The KPI is based on the relative ABA energy difference between the transition zones at the entrance side and the exit side of the bridge with respect to the travel direction of the measurement system. The KPI can be calculated as follows:

$$\text{KPI}^{\text{side}} = \frac{\left(\sum_{x=x_3}^{x_4} \overline{\text{SAWP}}^{\text{exit}}(x) - \sum_{x=x_1}^{x_2} \overline{\text{SAWP}}^{\text{entrance}}(x) \right)}{\frac{\left(\sum_{x=x_3}^{x_4} \overline{\text{SAWP}}^{\text{exit}}(x) + \sum_{x=x_1}^{x_2} \overline{\text{SAWP}}^{\text{entrance}}(x) \right)}{2}} \times 100$$

(7)

Table 3 KPI$^{\text{side}}$ to evaluate the relative degradation level between 2 transition zones

Direction	KPI$^{\text{side}}$			Interpretation
	Day 1	Day 2	Average	
To Murjek	44.06	43.30	43.68	The exit side transition zone (north abutment) is more degraded
To Boden	-6.61	-5.01	-5.81	The entrance side transition zone (north abutment) is more degraded

where $\sum_{x=x_m}^{x_n} \overline{\text{SAWP}}^{\text{location}}(x)$ is an average SAWP from four wheelsets at a considered location from x_m to x_n, x_1 and x_2 are the boundary positions of the transition zone at the entrance side, and x_3 and x_4 are the boundary positions of the transition zone at the exit side. A positive KPI$^{\text{side}}$ indicates that the transition zone at the exit site is more degraded. Based on the four measurements, the north abutment transition zone is more degraded than the south abutment, as shown in Table 3. The supporting reason is that the full loaded iron ore trains travel in the direction to Boden. The trains have the heaviest axle load that could accelerate the degradation of the north abutment transition zone.

4.2 Analysis of ABA features at transition zones

In this study, we consider investigating two extracted features from ABA signals: (1) the SAWP, which can be calculated according to Eqs. (3), and (2) the dominant frequency of a particular piece of track at a particular spatial frequency range, which can be defined as follows:

$$f_a^{dom}(x) = \arg\max_{f \in [f_1, f_2]} \left(\overline{GWPS}(f) \right), \quad x \in [x_1, x_2] \tag{8}$$

where $f_a^{dom}(x)$ is the dominant frequency in the range $a = [f_1, f_2]$ within the track location from x_1 to x_2, and $\overline{GWPS}(f)$ is an average GWPS from four wheelsets. In this study, we consider a moving window of 0.65 m with 95% overlap to capture the changes in the dominant frequency.

For a particular extracted feature, we considered its variation within two spatial frequency ranges. The first spatial frequency is between 0.04 m^{-1} and 0.33 m^{-1}, corresponding to wavelengths of 3 m to 25 m (D1 wavelength, according to EN 13848–1 [30]). The second range is between 1.05 m^{-1} and 2.86 m^{-1}, corresponding to wavelengths of 0.35 m to 0.95 m. This wavelength corresponds to the sleeper interval of ± 0.3 m. According to an investigation of the scalogram of the wavelet power spectrum, those two spatial frequency ranges provide the most noticeable ABA energy.

Figure 13 shows the variation in the ABA features measured on day 1 in the direction toward Murjek station, from -10 m to 10 m, covering the north transition zone and the bridge where impact tests are conducted. Besides the influence of the welds at − 7.7 m which obviously provide changes in ABA signals, in Fig. 13a and b, the dominant spatial frequency variation in the range of 0.04–0.33 m^{-1} (the green lines) of both rails shows a similar trend at the track segment on the bridge, where the dominant frequency gradually decreases from Zone A to Zone C, from 0.20 to 0.17 m^{-1}. In comparison, the track segment on the embankment from − 7 to − 2.5 m shows unevenness between the left and the right rails. Considering the dominant frequency in the range of 1.05–2.86 m^{-1} (the red lines), the dominant frequency is at 1.53 m^{-1} for most of the track locations on the right rail, and a slight shift occurs at the location of Zone C. In contrast, the dominant frequency on the left rail shows a higher level of fluctuation with a noticeable change from − 2 to 7 m. The highest shift is at 4.4 m in the middle of Zone B. Then, the dominant frequency gradually decreases to 1.53 m^{-1} at approximately 7 m in the middle of Zone C.

Variations in the SAWP from the left and right rails are shown in Fig. 13c and d. The SAWP in the range of 0.04–0.33 m^{-1} (the blue lines) gradually increases when approaching the bridge, with the highest value at about 2.0 m where is the connection between Zone A and Zone B (from the north abutment to the deck slab). Considering the SAWP in the range of 1.05–2.86 m^{-1} (the orange lines), the peaks due to the weld at − 7.7 m, which the right rail shows the higher magnitude, can be observed from the both rails. While the weld at − 0.3 m on the left rail does not provide significant peak. Besides, fluctuations in the SAWP
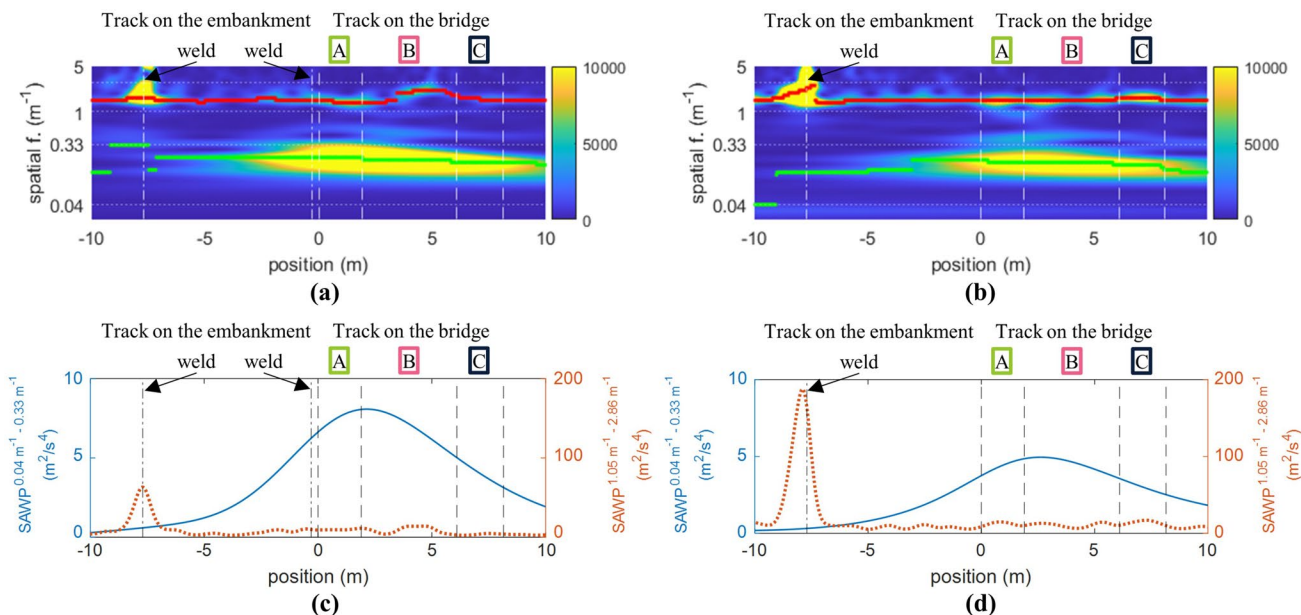

Fig. 13 Variation in the ABA features at the considered track segment: **a**, **b** dominant spatial frequencies on the left and right rails, ● corresponds to the range of 0.04 m^{-1} to 0.33 m^{-1}, ● corresponds to the range of 1.05 m^{-1} to 2.86 m^{-1}; **c**, **d** SAWP of 2 considered bands on the left and right rails

of both rails along the transition zones and the bridge can be observed.

According to these observations, a conclusion can be drawn that the considered ABA features are relevant to the variation in vertical track dynamic behavior. Noticeable changes are found at transition zones, in which the track support conditions change drastically. Furthermore, noticeable dissimilarities in ABA features between the left and right rails are found at some parts of the track. This indicates that there are differences in the local conditions between the rails.

4.3 Repeatability of the ABA measurements

This section evaluates the repeatability of the considered ABA features considering two measurement speeds and two measurement directions. Please note that the influence of the welds is not included in the analysis. Regarding the influence

of the measurement speed, the ABA signals from the left rail and measurements in the direction toward Murjek Station on Day 1, with a running speed of 31.7 m/s, and on Day 2, with a running speed of 33.7 m/s, are selected for evaluation. Figure 14a shows the considered ABA features from the two measurements. Both measurements show a similar pattern of dominant frequency in the ranges of 0.04–0.33 m^{-1} and 1.05–2.86 m^{-1}. The SAWPs from the two measurements are similar. However, the measurement with a higher measurement speed yields a higher SAWP magnitude than that with a slower measurement speed.

Next, the evaluation of the influence of the measurement directions is considered. The ABA signals on the left rail from the measurements in the direction toward Murjek Station on Day 2 with a measurement speed of 33.7 m/s and toward Boden Station on Day 2 with a measurement speed of 33.0 m/s are selected. Figure 14b shows the variation in the considered ABA features between the
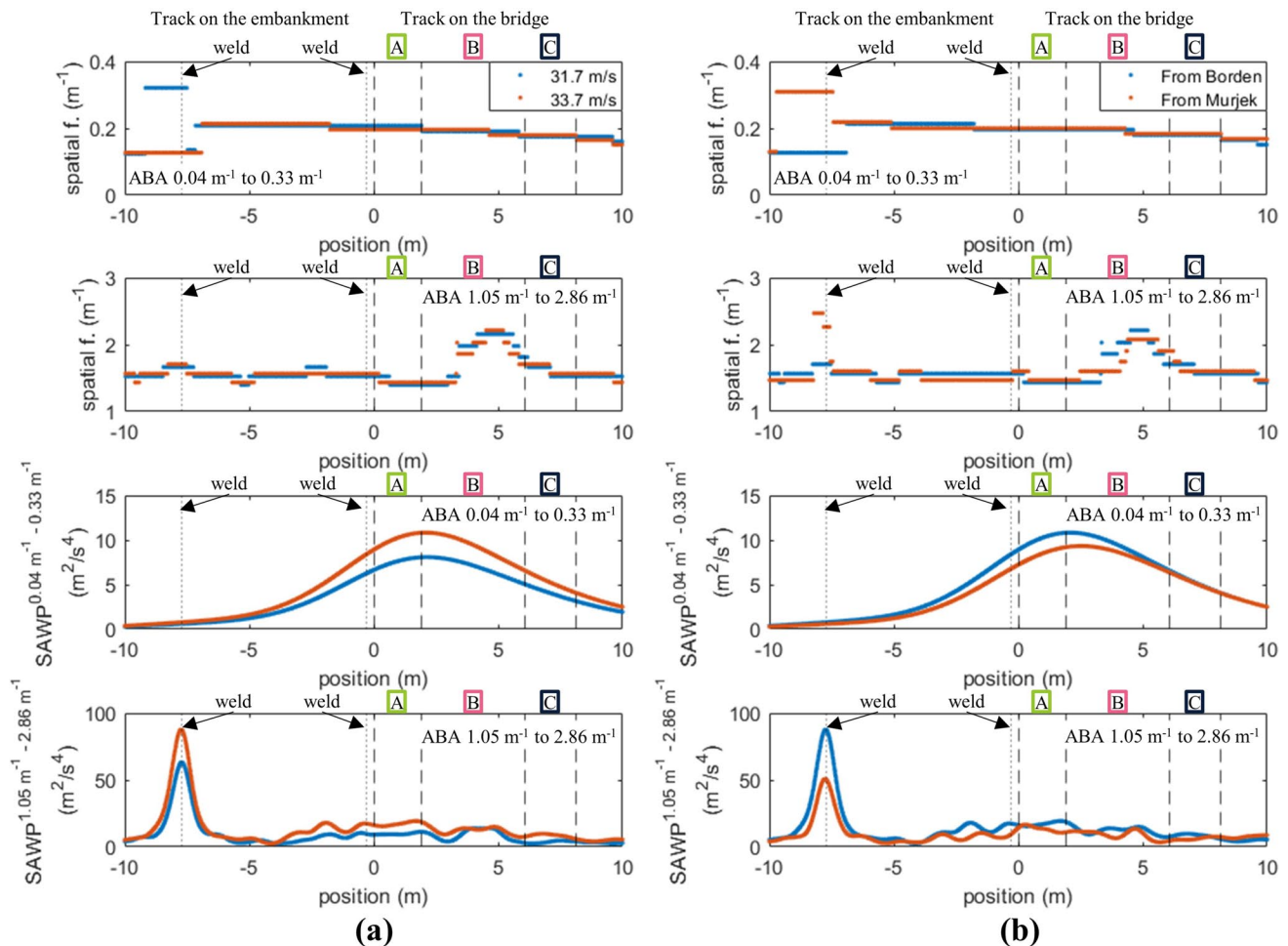
Fig. 14 Variation in the ABA features on the left rail: **a** different speeds; **b** different directions. The first and second rows are the dominant spatial frequencies in the ranges of 0.04–0.33 m^{-1} and

1.05–2.86 m^{-1}, respectively. The third and fourth rows are the SAWP corresponding to the dominant spatial frequency in the range of 0.04–0.33 m^{-1} and 1.05–2.86 m^{-1}, respectively

two measurements. Although the different wheel moving directions at the transition zones provide different wheel force distribution characteristics [1], the variations in the ABA features between the two measurements are similar. There are minor differences in ABA features in the range of 1.05–2.86 m^{-1} (see the second and the forth rows of Fig. 14b). The dominant frequencies show a slight difference in Zone B at approximately 4 m to 5 m from the middle of the bridge deck (the second row of Fig. 14b). Moreover, the SAWPs show different numbers of peaks and peak locations between − 3 and 5 m (the forth row of Fig. 14b).

These findings suggest that ABA measurements with different measurement speeds and directions provide considerable consistency ABA features. Making transition zone conditions monitoring using in-service trains more reliable.

5 Relationship between the impact tests and ABA measurement results

The results from the impact tests and ABA measurements allow us to estimate the variations in the vertical dynamic behavior at different locations in the transition zone. The
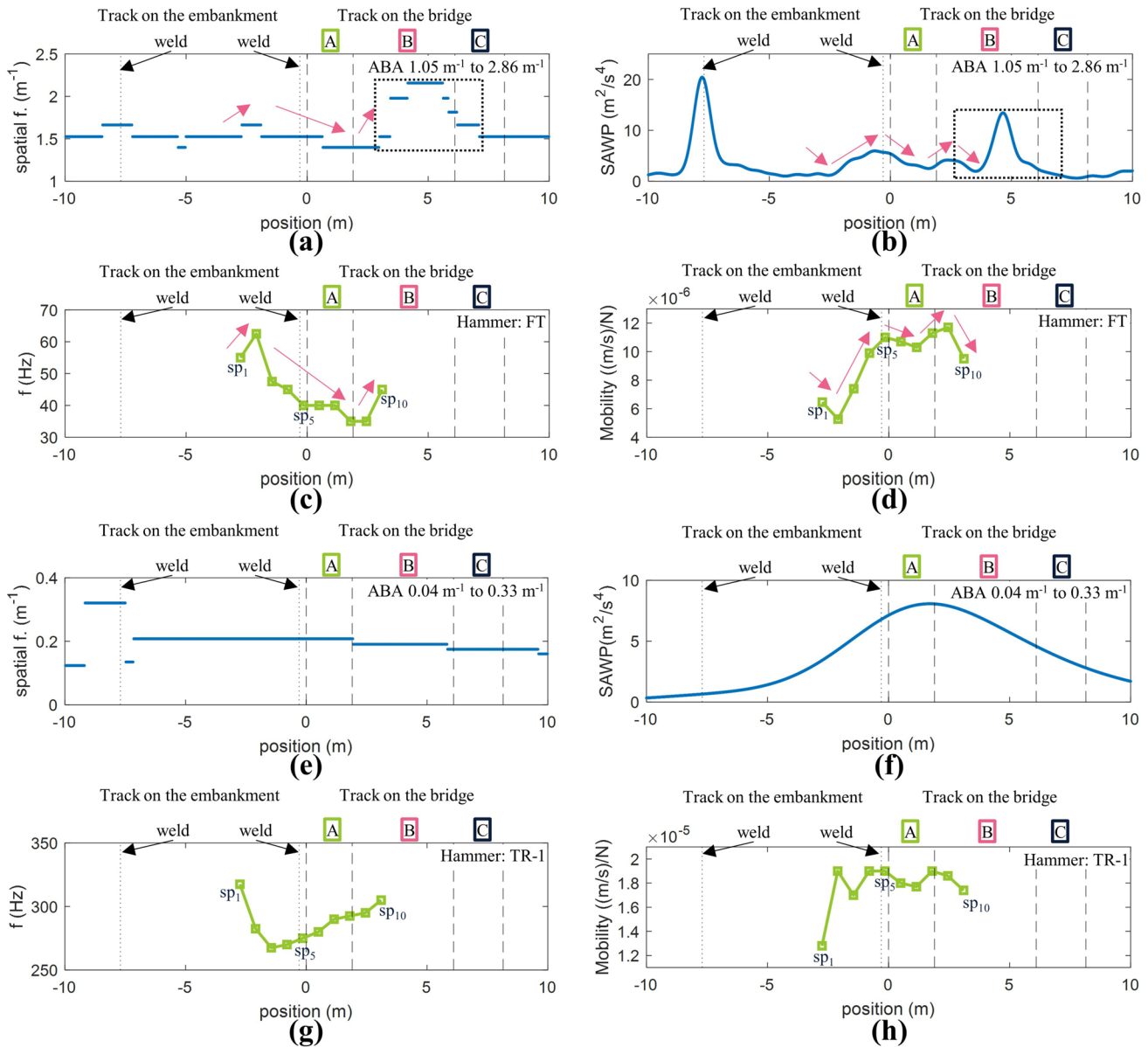
Fig. 15 The features from the hammer tests and ABA measurements: **a**, **b** the dominant frequency and SAWP in the range of 1.05–2.86 m^{-1}; **c**, **d** the FT resonance and its mobility magnitude; **e**, **f** the dominant frequency and SAWP in the range of 0.04–0.33 m^{-1}; **g**, **h** the TR-1 resonance and its mobility magnitude; □ indicates the positions of sleepers sp1–sp10, from left to right, respectively

proposed measurement framework can be used to assess the health conditions of railway tracks and estimate their properties, such as track stiffness and damping from FRF-derived features [17, 20, 22]. In this section, we analyze the possible relationships between the impact tests and ABA measurements to be able to interpret the condition monitoring results from ABA measurements.

The ABA responses in the ranges of 1.05–2.86 m^{-1} are most likely related to ballast layer conditions. An investigation shows that the changing trend of the dominant frequency of the ABA signals is aligned with the FT resonance obtained by the hammer tests, as shown in Fig. 15a and c. Both features show a decreasing trend from approximately − 2 m to the end of Zone A.

The SAWP from ABA signals follows a behavior similar to the FT resonance magnitude estimated from the hammer tests, as indicated by the arrows in Fig. 15b and d. An increasing trend of both features can be observed from approximately – 2–0 m. Then, both values fluctuate with two peaks from the beginning of Zone A to the beginning of Zone B.

These findings suggest that changes exist in the transition zone vertical dynamic behavior due to sleeper support conditions, in which conditions of a ballast layer are dominant. This finding agrees with the current knowledge that sleepers and rails vibrate together like a rigid body in terms of FT resonance, in which the properties of the ballast layer play a major role, as mentioned in Sect. 3.2.

In addition, the variation in the ABA features provides a noticeable change at 3.0 m to 7.0 m, which covers Zone B and Zone C, as shown in the dotted boxes in Fig. 15a and b. This region corresponds to the high deflection at the position of accelerometer a_6, according to the ODSs obtained with falling weight tests, as shown in Fig. 11. These high deflection factors could be a result of the ballast layer properties, and the location could be a contributing factor. This location is close to the middle span of the bridge deck, which tends to deflect and vibrate more than other parts.

Looking at Fig. 15e and f for the range of 0.04–0.33 m^{-1}, no clear relationship could be identified between the ABA responses and features from the hammer tests. ABA features in this range are not well aligned with the features of FT (Fig. 15c and d) and TR-1 (Fig. 15g and h) obtained by the hammer tests. The reason is that ABA responses in this range are related to the substructure condition in this spatial frequency range, while FT and TR-1 are related to the condition of the ballast layer and the components above it, respectively.

Even though the available measurement datasets from the impact tests cannot fully understand ABA features in the range of 0.04–0.33 m^{-1}, it has been reported that ABA responses in the spatial frequency range are related to the substructure conditions. Therefore, ABA measurements

still provide valuable insights into the conditions of the substructure and the ballast layer, allowing estimation of the health condition of the transition zone. Unlike a more degraded transition zone, a transition zone with healthy conditions should exhibit fewer fluctuations in its vertical dynamic characteristics. Notably, the ABA features near 0 m (the north abutment transition zone) show more pronounced changes compared to those near 8.15 m (the south abutment transition zone); please see Fig. 15a, b, e, and f. This observation suggests a higher degree of degradation in both the ballast and substructure layers in the north abutment transition zone, which aligns with the findings presented in Table 3.

6 Conclusions and suggestions for further works

This paper investigates the vertical dynamic behavior of a railway bridge transition zone through an experimental assessment with two measurement techniques: impact tests and onboard measurements. Impact tests provide information about some important track characteristics, including track resonant frequencies and their corresponding magnitudes, which can be observed from the FRFs from the hammer and falling weight tests. Additionally, the track deflection responses can be analyzed by means of the ODSs derived from falling weight tests. Moreover, ABA signal characteristics indicate that the variations in the train-track interactions at transition zones are strongly related to the track health condition. Since the two measurement techniques are based on different principles, analyzing the relationship between the features from the two techniques could provide more understanding of the ABA features. Furthermore, ABA measurements can be beneficial for health condition monitoring of transition zones at the network scale. According to the findings from the case study, the following conclusions can be drawn:

1. Variations in the FT and TR-1 resonances from hammer tests are observed at different transition zone locations. This indicates that different track vertical dynamic behaviors exist with respect to the ballast layer and the components above it. In comparison, an additional track resonance factor that is lower than FT can be obtained from the falling weight tests.
2. ODSs derived from the falling weight tests show different deflection characteristics along the transition zone. This indicates differences in vertical dynamic responses between segments of the track on the embankment and the track on the bridge.
3. The ABA features from different operational conditions, which are the speeds and moving directions, show con-

siderable consistency in the dominant frequencies and SAWPs along the transition zone, particularly in the two considered spatial frequency ranges, 0.04–0.33 m^{-1} and 1.05–2.86 m^{-1}. This knowledge can be utilized to minimize the influence of uncertainty in transition zone condition monitoring with in-service trains.

4. The ABA features in the spatial frequency range of 1.05–2.86 m^{-1} are related to ballast layer conditions since a similar pattern can be observed between the ABA features and FT resonance features. The dominant ABA frequency is related to the FT resonant frequency, while the SAWP of the ABA is related to the magnitude of the FT resonance.

5. The location that is highly deflected due to excitation can be identified by both ABA measurement and falling weight tests, and the results from both measurement techniques are well aligned.

In further works, additional extensive falling weight tests should be conducted to link its corresponding FRF features, which are expected to be related to substructure components, with ABA features in the range of 0.04–0.33 m^{-1}. The finding could support a statement that track irregularities in this frequency range are related to substructure component conditions. Part of the further research will include analyzing the relationship between the ABA responses and other track inspection techniques, such as ground penetrating radar (GPR) and track geometry measurements, which can provide a better understanding of the ABA responses concerning various aspects of the track characteristics.

Data availability Data availability upon request to z.li@tudelft.nl.

References

1. Sañudo R, Dell'Olio L, Casado JA, Carrascal IA, Diego S (2016) Track transitions in railways: a review. Constr Build Mater 112:140–157. https://doi.org/10.1016/j.conbuildmat.2016.02.084

2. Wang H, Markine V (2019) Dynamic behaviour of the track in transitions zones considering the differential settlement. J Sound Vib 459:114863. https://doi.org/10.1016/j.jsv.2019.114863

3. Bezin Y, Iwnicki SD, Cavalletti M, de Vries E, Shahzad F, G, (2009) Evans, an investigation of sleeper voids using a flexible track model integrated with railway multi-body dynamics. Proc Inst Mech Eng Part F J Rail Rapid Transit 223:597–607. https://doi.org/10.1243/09544097JRRT276

4. Zhu JY, Thompson DJ, Jones CJC (2011) On the effect of unsupported sleepers on the dynamic behaviour of a railway track. Veh Syst Dyn 49:1389–1408. https://doi.org/10.1080/00423114.2010.524303

5. Ang KK, Dai J (2013) Response analysis of high-speed rail system accounting for abrupt change of foundation stiffness. J Sound Vib 332:2954–2970. https://doi.org/10.1016/j.jsv.2013.01.005

6. T. Dahlberg (2003), Railway track settlements-a literature review. Report for the EU project SUPERTRACK—Linkoping University Sweden. http://www-classes.usc.edu/engr/ce/599/Thesis/RTRSETTL.pdf

7. Auersch L (2022) Different types of continuous track irregularities as sources of train-induced ground vibration and the importance of the random variation of the track support. Appl Sci 12:1463. https://doi.org/10.3390/app12031463

8. Auersch L (2015) Excitation of ground vibration due to the passage of trains over a track with trackbed irregularities and a varying support stiffness. Veh Syst Dyn 53:1–29. https://doi.org/10.1080/00423114.2014.968173

9. Hölscher P, Meijers P (2007) Literature study of knowledge and experience of transition zones

10. Rose JG, Stark TD, Wilk ST, Purcell M (2015) Design and monitoring of well-performing bridge transitions. In: 2015 Jt. Rail Conf., American Society of Mechanical Engineers. https://doi.org/10.1115/JRC2015-5645.

11. Alves Ribeiro C, Calçada R, Delgado R (2017) Experimental assessment of the dynamic behaviour of the train-track system at a culvert transition zone. Eng Struct 138:215–228. https://doi.org/10.1016/j.engstruct.2017.02.020

12. Stark TD, Wilk ST (2016) Root cause of differential movement at bridge transition zones. Proc Inst Mech Eng Part F J Rail Rapid Transit 230:1257–1269. https://doi.org/10.1177/0954409715589620

13. Mishra D, Tutumluer E, Boler H, Hyslip JP, Sussmann TR (2014) Railroad track transitions with multidepth deflectometers and strain gauges. Transp Res Rec J Transp Res Board 2448:105–114. https://doi.org/10.3141/2448-13

14. Rodríguez A, Sañudo R, Miranda M, Gómez A, Benavente J (2021) Smartphones and tablets applications in railways, ride comfort and track quality. Transition zones analysis. Measurement 182:109644. https://doi.org/10.1016/j.measurement.2021.109644

15. Wang H, Berkers J, van den Hurk N, Layegh NF (2021) Study of loaded versus unloaded measurements in railway track inspection. Measurement 169:108556. https://doi.org/10.1016/j.measurement.2020.108556

16. Unsiwilai S, Wang L, Núñez A, Li Z (2023) Multiple-axle box acceleration measurements at railway transition zones. Measurement 213:112688. https://doi.org/10.1016/j.measurement.2023.112688

17. Oregui M, Li Z, Dollevoet R (2015) Identification of characteristic frequencies of damaged railway tracks using field hammer test measurements. Mech Syst Signal Process 54:224–242. https://doi.org/10.1016/j.ymssp.2014.08.024

18. Oregui M, Molodova M, Núñez A, Dollevoet R, Li Z (2015) Experimental investigation into the condition of insulated rail joints by impact excitation. Exp Mech 55:1597–1612. https://doi.org/10.1007/s11340-015-0048-7

19. Xiong Z, Liu J, Wang P, Liu G, Xiao J, Yu S (2021) Field dynamic performance testing and analysis of polyurethane track and ballasted track in a high-speed railway. J Civ Struct Heal Monit 11:867–877. https://doi.org/10.1007/s13349-021-00489-6

20. Shen C, Dollevoet R, Li Z (2021) Fast and robust identification of railway track stiffness from simple field measurement. Mech Syst Signal Process 152:107431. https://doi.org/10.1016/j.ymssp.2020.107431

21. Oregui M, Li Z, Dollevoet R (2015) An investigation into the modeling of railway fastening. Int J Mech Sci 92:1–11. https://doi.org/10.1016/j.ijmecsci.2014.11.019

22. De Man AP (2002) DYNATRACK: a survey of dynamic railway track properties and their quality. Delft Univ. Technol, TU Delft

23. Knothe K, Wu Y (1998) Receptance behaviour of railway track and subgrade. Arch Appl Mech 68:457–470. https://doi.org/10.1007/s004190050179

24. Wei Z, Boogaard A, Nunez A, Li Z, Dollevoet R (2018) An integrated approach for characterizing the dynamic behavior of the wheel-rail interaction at crossings. IEEE Trans Instrum Meas 67:2332–2344. https://doi.org/10.1109/TIM.2018.2816800

25. Li Z, Molodova M, Nunez A, Dollevoet R (2015) Improvements in axle box acceleration measurements for the detection of light squats in railway infrastructure. IEEE Trans Ind Electron 62:4385–4397. https://doi.org/10.1109/TIE.2015.2389761

26. Molodova M, Oregui M, Núñez A, Li Z, Dollevoet R (2016) Health condition monitoring of insulated joints based on axle box acceleration measurements. Eng Struct 123:225–235. https://doi.org/10.1016/j.engstruct.2016.05.018

27. Torrence C, Compo GP (1998) A practical guide to wavelet analysis. Bull Am Meteorol Soc 79:61–78. https://doi.org/10.1175/1520-0477(1998)079%3c0061:APGTWA%3e2.0.CO;2

28. Knothe K, Grassie SL (1993) Modelling of railway track and vehicle/track interaction at high frequencies. Veh Syst Dyn 22:209–262. https://doi.org/10.1080/00423119308969027

29. Schwarz BJ, Richardson MH (1999) Introduction to operating deflection shapes. CSI Reliab Week 10:121–126

30. CEN (2019) NEN-EN 13848-1:2019 en—Railway applications—track—track geometry quality—part 1: characterization of track geometry. https://www.nen.nl/en/nen-en-13848-1-2019-en-257518

Publisher's Note Springer Nature remains neutral with regard to jurisdictional claims in published maps and institutional affiliations.